International Journal of Nanomedicine

Dovepress
open access to scientific and medical research

Open Access Full Text Article

ORIGINAL RESEARCH

Asymmetric dumbbell-shaped silver nanoparticles and spherical gold nanoparticles green-synthesized by mangosteen (*Garcinia mangostana*) pericarp waste extracts

This article was published in the following Dove Press journal:
International Journal of Nanomedicine
14 September 2017
Number of times this article has been viewed

Ji Su Park
Eun-Young Ahn
Youmie Park

College of Pharmacy, Inje Institute of Pharmaceutical Sciences and Research, Inje University, Gimhae, Gyeongnam, Republic of Korea

Abstract: Mangosteen (*Garcinia mangostana*) pericarp waste extract was used to synthesize gold and silver nanoparticles by a green strategy. The extract was both a reducing and stabilizing agent during synthesis. Phytochemical screening of the extract was conducted to obtain information regarding the presence/absence of primary and secondary metabolites in the extract. The in vitro antioxidant activity results demonstrated that the extract had excellent antioxidant activity, which was comparable to a standard (butylated hydroxy toluene). Spherical gold nanoparticles (gold nanoparticles green synthesized by mangosteen pericarp extract [GM-AuNPs]) with an average size of 15.37±3.99 to 44.20±16.99 nm were observed in high-resolution transmission electron microscopy (HR-TEM) images. Most interestingly, the silver nanoparticles (silver nanoparticles green synthesized by mangosteen pericarp extract [GM-AgNPs]) had asymmetric nanodumbbell shapes where one tail grew from a spherical head. The average head size was measured to be 13.65±5.07 to 31.08±3.99 nm from HR-TEM images. The hydrodynamic size of both nanoparticles tended to increase with increasing extract concentration. Large negative zeta potentials (−18.92 to −34.77 mV) suggested that each nanoparticle solution possessed excellent colloidal stability. The reaction yields were 99.7% for GM-AuNPs and 82.8% for GM-AgNPs, which were assessed by inductively coupled plasma optical emission spectroscopy. A high-resolution X-ray diffraction pattern confirmed the face-centered cubic structure of both nanoparticles. Based on phytochemical screening and Fourier transform infrared spectra, the hydroxyl functional groups of carbohydrates, flavonoids, glycosides, and phenolic compounds were most likely involved in a reduction reaction of gold or silver salts to their corresponding nanoparticles. The in vitro cytotoxicity (based on a water-soluble tetrazolium assay) demonstrated that GM-AgNPs were toxic to both A549 (a human lung cancer cell) and NIH3T3 (a mouse fibroblast cell). The cytotoxicity of GM-AgNPs on A549 cells was related to apoptotic cell death. However, GM-AuNPs did not show any significant cytotoxicity to either cell. These results suggest that GM-AuNPs have the potential to be drug delivery vehicles or carriers for pharmaceutical and biomedical applications.

Keywords: mangosteen pericarp extracts, *Garcinia mangostana*, green synthesis, gold nanoparticles, silver nanoparticles, asymmetric silver nanodumbbells, cytotoxicity, apoptosis, A549 human lung cancer cell, NIH3T3 mouse fibroblast cell

Correspondence: Youmie Park
College of Pharmacy, Inje Institute of Pharmaceutical Sciences and Research, Inje University, 197 Inje-ro, Gimhae, Gyeongnam 50834, Republic of Korea
Tel +82 55 320 3884
Fax +82 55 320 3940
Email youmiep@inje.ac.kr

Introduction

Currently, metallic nanoparticles have received great attention due to their characteristic physical and chemical properties when compared with their bulk counterparts.

submit your manuscript | www.dovepress.com
Dovepress
http://dx.doi.org/10.2147/IJN.S140190

Gold nanoparticles (AuNPs) have been widely applied for drug delivery, photothermal cancer therapy, chemical and biological sensing, imaging, and catalysis.[1–3] Silver nanoparticles (AgNPs) have been extensively used in antimicrobial applications, specifically, as antibacterial agents.[4,5] The traditional synthesis of AuNPs involves the use of chemical reducing agents to convert metal salts to metallic nanoparticles via a reduction reaction. Currently, global sustainability initiatives have been focal issues for the synthesis of metallic nanoparticles. In recent years, the use of noxious chemicals as reducing agents has been eliminated, and plant extracts have replaced these chemicals to protect public health and the global environment. There are extensive reviews elsewhere regarding the use of plant extracts as reducing agents.[6] This green (or eco-friendly or sustainable) synthetic strategy has the following advantages: 1) the reaction is facile and simple; 2) the reaction can be carried out in a one-pot and one-step process; 3) it is amenable to scale-up for mass production; and 4) finally, synergistic biological effects of the resulting metallic nanoparticles can be expected by combining the intrinsic activities of plant extracts and metallic nanoparticles. Generally, plant extracts possessing intrinsic biological properties, such as antimicrobial, antioxidant, anti-inflammatory, and anticancer activities, have been selected to reinforce the activities of the resulting metallic nanoparticles.

Mangosteen (*Garcinia mangostana* L., Clusiaceae) is a tropical fruit known as "the queen of fruits".[7] Mangosteen has been used as a traditional medicine in Southeast Asia and possesses biologically active compounds, including phenolic acids, xanthones, tannins, and anthocyannins.[7] Currently, mangosteen is popular as a botanical dietary supplement. Mangosteen has antioxidant, antibacterial, antifungal, anti-inflammatory, and anti-HIV activities in vitro.[8] Mangosteen also exhibits central nervous system depressant, anti-inflammatory, and antiulcer activities in vivo.[8] Suttirak and Manurakchinakorn[7] reported that antioxidant activity of mangosteen pericarp extract is affected by several factors as follows: 1) during the maturation stage, young fruit pericarp has higher concentrations of total phenolics and total tannins, while mature fruit pericarp contains higher total flavonoid content; 2) in the extraction solvent, the antioxidant activity is dependent on the solvents that are used for extraction due to the different solvent polarities that result with different contents of compounds in the extracted material; and 3) in the material preparation, generally, mangosteen pericarp is subjected to a drying step, and the xanthone content and free radical scavenging activity are affected by drying methods, which cause either enzymatic or thermal degradation of xanthones.

There are several research articles regarding the green synthesis of AgNPs using mangosteen leaf and fruit extracts.[9–11] The synthesized AgNPs showed antibacterial and antioxidant activities. In other reports, polymers were employed for the preparation of nanoparticles containing mangosteen extracts.[12–14] Cellulose and Eudragit (polymethacrylate-based copolymers) were used to encapsulate mangosteen extracts. These polymeric nanoparticles exhibited anticancer and anti-*Helicobacter pylori* activities.

Mangosteen is composed of two major parts. One is the edible aril, and the other is the pericarp.[7] As a food source, people usually consume the aril part, whereas the pericarp is a waste.[7] In the present report, the methanol extract of mangosteen pericarp was utilized as a valuable reducing agent for the green synthesis of AuNPs (referred to hereafter as GM-AuNPs) and AgNPs (referred to hereafter as GM-AgNPs). Therefore, this synthetic strategy is totally green, eco-friendly, and sustainable for the following reasons: 1) during the synthetic process, no other chemicals were employed except the extract as a reducing agent; 2) the pericarp waste was utilized as a valuable reducing agent; and 3) water was used as a solvent instead of organic solvents during synthesis. Before synthesizing GM-AuNPs and GM-AgNPs, we performed phytochemical screening (20 tests in Table 1) and in vitro antioxidant activity assays of the extract. Moreover, the contents of total phenolic compounds and reducing sugars were quantified in the extract. For the synthesis of

Table 1 Phytochemical screening of the extract (+, present; –, absent)

Phytochemicals	Screening tests	Presence or absence of phytochemicals
Alkaloids	Mayer's test	–
	Wagner's test	+
	Hager's test	–
	Tannic acid test	–
Amino acids	Ninhydrin test	–
Carbohydrates	Molisch's test	+
	Fehling's test	+
Flavonoids	Alkaline reagent test	+
	Lead acetate test	+
Glycosides	General test	+
Anthraquinone glycosides	Modified Borntrager's test	–
	Hydroxyanthraquinone test	+
Cardiac glycosides	Baljet's test	–
	Keller–Killiani test	–
Saponins	Froth test	+
Phenolic compounds	Gelatin test	+
	Ferric chloride test	+
Phytosterols	Liebermann–Burchard's test	+
	Salkowski's test	+
Diterpenes	Copper acetate test	+

GM-AuNPs and GM-AgNPs, eight different extract concentrations were varied from 0.02% to 0.09% under a fixed concentration of metal salts during the synthesis. The sizes and shapes of the prepared GM-AuNPs and GM-AgNPs were characterized by high-resolution transmission electron microscopy (HR-TEM). Additionally, the hydrodynamic size and zeta potential values were also measured. Subsequently, GM-AuNPs and GM-AgNPs that were synthesized with the lowest extract concentration (0.02%) were further characterized by high-resolution X-ray diffraction (HR-XRD) and Fourier transform infrared spectroscopy (FT-IR). The reaction yield was assessed by using inductively coupled plasma optical emission spectroscopy (ICP-OES). Finally, the in vitro cytotoxicity and apoptosis toward A549 (a human lung cancer cell) and NIH3T3 (a mouse fibroblast cell) were evaluated using the water-soluble tetrazolium (WST) assay and Annexin V/propidium iodide (PI) staining to explore the potential applications of these nanoparticles in biomedical and pharmaceutical applications.

Materials and methods

Materials

Hydrochloroauric acid trihydrate ($HAuCl_4 \cdot 3H_2O$), silver nitrate, copper(II) acetate, mercury(II) chloride, potassium iodide, tannic acid, ninhydrin, α-naphthol, Folin–Ciocalteu's phenol reagent, sodium hydroxide, hydrochloric acid, lead acetate trihydrate, iron(II) chloride tetrahydrate, ammonia solution, acetic acid, sulfuric acid, gelatin solution, sodium chloride, sodium carbonate, gallic acid, potassium sodium tartrate, sodium bicarbonate, D-(+)-glucose, 2,6-di-*tert*-butyl-4-methylphenol (dibutyl hydroxyl toluene, butylated hydroxy toluene [BHT]), 2,2′-azino-bis(3-ethylbenzothiazoline-6-sulfonic acid) (ABTS) diammonium salt, potassium persulfate, sodium nitroprusside, sodium phosphate monobasic, sodium phosphate dibasic, sulfanilamide, nitrotetrazolium blue chloride, and phenazine methosulfate were purchased from Sigma-Aldrich (St Louis, MO, USA). *N*-(1-Naphthyl) ethylenediamine dihydrochloride, Fehling's reagent I, and Fehling's reagent II were obtained from Fluka (St Louis, MO, USA). 2,2-Diphenyl-1-picrylhydrazyl (DPPH) was from Alfa Aesar (Heysham, England). Iodine, potassium hydroxide, and iron(III) chloride were purchased from Duksan (Gyeonggi, Republic of Korea). Picric acid was obtained from Applichem Panreac (Gatersleben, Saxony-Anhalt, Germany). Sodium sulfate, hexaammonium heptamolybdate tetrahydrate, and disodium hydrogen arsenate heptahydrate were purchased from Junsei (Tokyo, Japan). Copper sulfate pentahydrate was obtained from Daejung (Gyeonggi, Republic of Korea). Nicotinamide adenine dinucleotide reduced from (NADH) was from Roche (Basel, Switzerland). Chloroform was obtained from Burdick & Jackson (Ulsan, Republic of Korea). Ethanol and methanol were from SK Chemical (Gyeonggi, Republic of Korea). For the in vitro cytotoxicity assay (WST assay), the EZ-CYTOX assay kit was obtained from DoGenBio (Gyeonggi, Republic of Korea). The Annexin V–fluorescein isothiocyanate (FITC)/PI apoptosis detection kit (BD Biosciences, San Jose, CA, USA) was utilized to observe the apoptotic effect. Both A549 and NIH3T3 cells were purchased from the Korean Cell Line Bank (Seoul, Republic of Korea). All other reagents were of analytical grade. Deionized water was used for the preparation of all the solutions.

Instruments

Ultraviolet (UV)-visible spectra were recorded using a Shimadzu UV-1800 or a Shimadzu UV-2600 to observe the surface plasmon resonance (SPR) of metallic nanoparticles (Shimadzu Corporation, Kyoto, Japan). The sizes and shapes of the nanoparticles were analyzed by obtaining HR-TEM images. Either a JEM-3010 or a JEM-2100F operated at 300 or 200 kV, respectively, was used to obtain HR-TEM images (JEOL, Tokyo, Japan). A carbon-coated copper grid (carbon type-B, 300 mesh; Ted Pella, Redding, CA, USA) was used for loading the nanoparticle solution, and the sample-loaded grid was air-dried. The hydrodynamic size along with polydispersity index was measured by dynamic light scattering on a NanoBrook 90Plus Zeta at 25°C (Brookhaven Instruments Co., Holtsville, NY, USA). Zeta potential values were also measured on this system at 25°C. The HR-XRD pattern was acquired to confirm the crystalline nature of the nanoparticles on a Bruker D8 Discover high-resolution X-ray diffractometer with a CuKα radiation source ($\lambda = 0.154056$ nm) in the range of 20°–90° (2θ scale) (Bruker Optik GmbH, Ettlingen, Germany). FT-IR spectra were obtained on a Varian 640 IR in attenuated total reflectance mode (Agilent Technologies, Palo Alto, CA, USA). The lyophilized samples were prepared using a FD5505 freeze dryer (Il Shin Bio, Seoul, Republic of Korea).

Extraction procedure of mangosteen pericarp

Frozen mangosteens were originally imported from Thailand and purchased from a local food market (Gimhae, Gyeongnam, Republic of Korea). The aril part was consumed, and the pericarp was collected. The pericarp was washed with deionized water, made into small pieces, and dried in a 50°C oven. After drying, the powdered sample of mangosteen pericarp

was prepared using a blender. The powdered sample (1.13 kg) was mixed with methanol in a volume ratio of sample/methanol =1/3. The extraction was performed at 50°C for 2 h with a sonicator WUC-A22H (Daihan Scientific Co. Ltd., Seoul, Republic of Korea). The extraction step was repeated three times, and a methanol crude extract (weight 339 g) was obtained by evaporating the solvent under reduced pressure. The methanol crude extract (weight 78 g) was redissolved in water, sonicated for 2 h, and centrifuged (685× *g* force, 20°C, 30 min). The supernatant was filtered through a 0.2 μm polytetrafluoroethylene (PTFE) syringe filter and freeze-dried (weight 65 g). This material was labeled "mangosteen pericarp extract" and redissolved in deionized water to prepare a stock solution (2%, w/v). This material was used for phytochemical screening, quantification of total phenolic compounds and reducing sugars, in vitro antioxidant activity, and the synthesis of GM-AuNPs and GM-AgNPs as discussed in the following sections.

Green synthesis of GM-AuNPs and GM-AgNPs

For the synthesis of GM-AuNPs, the mixture was prepared by combining hydrochloroauric acid trihydrate (10 mM, 105 μL) and the extract (2%, 30–135 μL). The final volume was adjusted to 3 mL by adding deionized water. Then, the mixture was vortexed for 5 s and incubated at ambient temperature for 5 h. The final concentrations of hydrochloroauric acid trihydrate and the extract were 0.35 mM and 0.02%–0.09%, respectively. In the case of GM-AgNPs, silver nitrate (10 mM, 105 μL) was used instead of hydrochloroauric acid trihydrate (10 mM, 105 μL) in the aforementioned procedure. All other reaction conditions of GM-AgNPs were the same as for the synthesis of GM-AuNPs.

Phytochemical screening, total phenolic content, reducing sugar content, and in vitro antioxidant activity of the extract

After obtaining the mangosteen pericarp extract in the previous section, the phytochemical screening was performed according to previous reports.[15,16] Twenty tests were carried out, as shown in Table 1. The total phenolic compound and reducing sugar contents were analyzed according to previous reports.[17,18] In vitro antioxidant activity, including DPPH, ABTS, nitric oxide, and superoxide anion radical scavenging activities, was also investigated according to previous reports.[19–22]

Assessment of reaction yield by using ICP-OES

The reaction yield was assessed by using ICP-OES (Optima 8300 ICP-OES, PerkinElmer Inc., Waltham, MA, USA). Both GM-AuNPs and GM-AgNPs were synthesized with 0.02% extract concentration. The detailed procedure of synthesis was mentioned in the previous section. Each colloidal solution was centrifuged at 18,410× *g* force for 7 h. The supernatant containing unreacted Au ion or Ag ion was pooled and submitted to ICP-OES analyses along with each colloidal solution.

In vitro cytotoxicity

The in vitro cytotoxicity of GM-AuNPs and GM-AgNPs was assessed by the WST assay on A549 and NIH3T3 cells. Both nanoparticle colloidal solutions were concentrated to 30-fold by using a vacuum evaporator. On 96-well plates, the cells were seeded at a density of 5.0×10^3 cells/well. Then, the incubation was conducted for 24 h in an oven at 37°C under a CO_2 (5%) atmosphere. Next, different concentrations of GM-AuNPs and GM-AgNPs (0, 18.75, 37.5, and 75 μg/mL, based on the extract concentration) were treated and incubated in the oven for 24 h at 37°C under a CO_2 (5%) atmosphere. The WST reagent (10 μL) from the EZ-CYTOX kit was added and incubated in the oven for an additional 1 h. The absorbance was measured at 450 nm using a microplate reader (Synergy HT; BioTek, Winooski, VT, USA). The intrinsic absorbance of GM-AuNPs and GM-AgNPs interfered with the measurement of cytotoxicity at 450 nm. Thus, the cytotoxicity was obtained by subtracting the background absorbance of GM-AuNPs and GM-AgNPs. The background absorbance was measured in a cell-free condition. The untreated cells were utilized as a control.

Cell morphological observation

Both A549 and NIH3T3 cells (0.3×10^6 cells/well) were seeded separately in six-well plates and were left to adhere for 24 h. Then the cells were treated with three samples (ie, the extract, GM-AuNPs, and GM-AgNPs) the concentration of which was 37.5 μg/mL (based on the extract concentration). After incubation for 24 h, the cells were viewed with inverted tissue culture microscope photographs taken by a CK40-32PH inverted microscope (Olympus,Tokyo, Japan) at a magnification of ×200.

Annexin V/PI staining

Apoptotic cells were discerned from necrotic and viable cells by being stained with Annexin V-FITC and PI.[23] Each cell (A549 and NIH3T3, 0.3×10^6 cells/well) was seeded in six-well plates and cultured for 24 h. Then three samples (ie, the extract, GM-AuNPs, and GM-AgNPs) were treated with various concentrations (0, 18.75, 37.5, and 75 μg/mL, based on the extract concentration). After 24 h incubation,

the cells were collected by trypsinization, washed with cold PBS, and subsequently centrifuged. The pellet was suspended in binding buffer (100 µL) and stained with Annexin V-FITC (5 µL) and PI (5 µL of 50 µg/mL) for 25 min at ambient temperature in the dark. The cells were analyzed with a FACS Calibur flow cytometer (BD Biosciences). In each analysis, 10,000 gate events were recorded. Analyses were performed by CellQuest software (BD, Franklin Lakes, NJ, USA), which provided information about apoptotic cells (%).

Statistical analysis

All experiments were performed in triplicate. Values were exported to Excel and presented as mean (standard deviation). To demonstrate variations, one-way ANOVA test was performed using Microsoft Excel "Analysis Toolpak" program. Statistical significance was determined by Student's *t*-test in the same program.

Results and discussion

Phytochemical screening of the extract

Phytochemical screening was carried out to investigate the primary and secondary metabolites in the extract. This process, along with FT-IR spectroscopy, is important to determine which of the compounds are involved in the synthesis of nanoparticles. Rajakannu et al[11] have reported on the phytochemical screening of the fruit extract of *G. mangostana*. According to their report, primary and secondary metabolites present in the water extract were tannins, saponins, flavonoids, proteins, steroids, anthraquinones, phenols, carbohydrates, and ascorbic acid. Phytochemical screening of the extract used for the synthesis of GM-AuNPs and GM-AgNPs in the current report was conducted, and the results are presented in Table 1. The primary and secondary metabolites present in the extract were alkaloids, carbohydrates, flavonoids, glycosides, anthraquinone glycosides, saponins, phenolic compounds, phytosterols, and diterpenes. Generally, phenolic compounds and flavonoids have been known as major contributors to the antioxidant activity of the extract.[24] Therefore, based on our phytochemical screening, it is most likely that phenolic compounds and flavonoids endow the extract with reducing properties and lead to the successful synthesis of GM-AuNPs and GM-AgNPs.

In vitro antioxidant activity, total phenolic compound, and reducing sugar contents of the extract

Mangosteen pericarp is a significant source of natural antioxidants. In vitro antioxidant assays were performed on the extract, and the resulting IC_{50} values are summarized in Table 2; the assays used were as follows: DPPH radical scavenging, ABTS radical scavenging, nitric oxide radical scavenging, and superoxide anion radical scavenging activities. BHT was used as a positive control. Except ABTS radical scavenging activity (extract IC_{50} 14.14 µg/mL), the extract exhibited lower IC_{50} values in DPPH radical scavenging (extract IC_{50} 26.44 µg/mL), nitric oxide radical scavenging (extract IC_{50} 70.59 µg/mL), and superoxide anion radical scavenging activities (extract IC_{50} 32.81 µg/mL) than BHT. This result suggests that the extract has excellent antioxidant activity.

Table 2 In vitro antioxidant activity of the extract (IC_{50}, µg/mL)

	DPPH radical scavenging	ABTS radical scavenging	Nitric oxide radical scavenging	Superoxide anion radical scavenging
Extract	26.44	14.14	70.59	32.81
Standard (BHT)	62.30	3.92	518.46	162.41

Abbreviations: ABTS, 2,2′-azino-bis(3-ethylbenzothiazoline-6-sulfonic acid); BHT, butylated hydroxy toluene; DPPH, 2,2-diphenyl-1-picrylhydrazyl.

Next, the total phenolic compound content was analyzed using the Folin–Ciocalteu method.[17] Gallic acid was used as a standard, and a calibration curve was constructed ($y = 5.2138x + 0.1116$, $r^2 = 0.999$) (data not shown). The total phenolic compound content was found to be 0.195 mg gallic acid equivalents (GAE)/1 mg extract. The reducing sugar content was also measured using the Nelson–Somogyi method with glucose as a standard.[17] A calibration curve for glucose was constructed ($y = 0.002x - 0.216$, $r^2 = 0.982$) (data not shown). The reducing sugar content was measured to be 0.903 mg glucose/1 mg extract.

Green synthesis of GM-AuNPs and GM-AgNPs with different extract concentrations

The extract concentration was varied from 0.02% to 0.09% while maintaining final concentrations of hydrochloroauric acid trihydrate and silver nitrate at 0.35 mM. UV-visible spectra were generally recorded to follow the reaction progress and monitor the reaction completion. UV-visible spectra of the resulting GM-AuNPs (Figure 1A) and GM-AgNPs (Figure 1B) are shown. Under the lowest concentration of the extract (0.02%), GM-AuNPs showed two SPR bands near 700 nm and at 800–1,000 nm. The broad band at 800–1,000 nm was blue-shifted close to 700 nm when the extract concentration was increased to 0.03%. When the concentration was higher than 0.03%, only one SPR band at 500–600 nm was observed in GM-AuNPs (Figure 1A). The characteristic SPR signal of the AgNPs appeared at 400–500 nm in GM-AgNPs synthesized with all extract

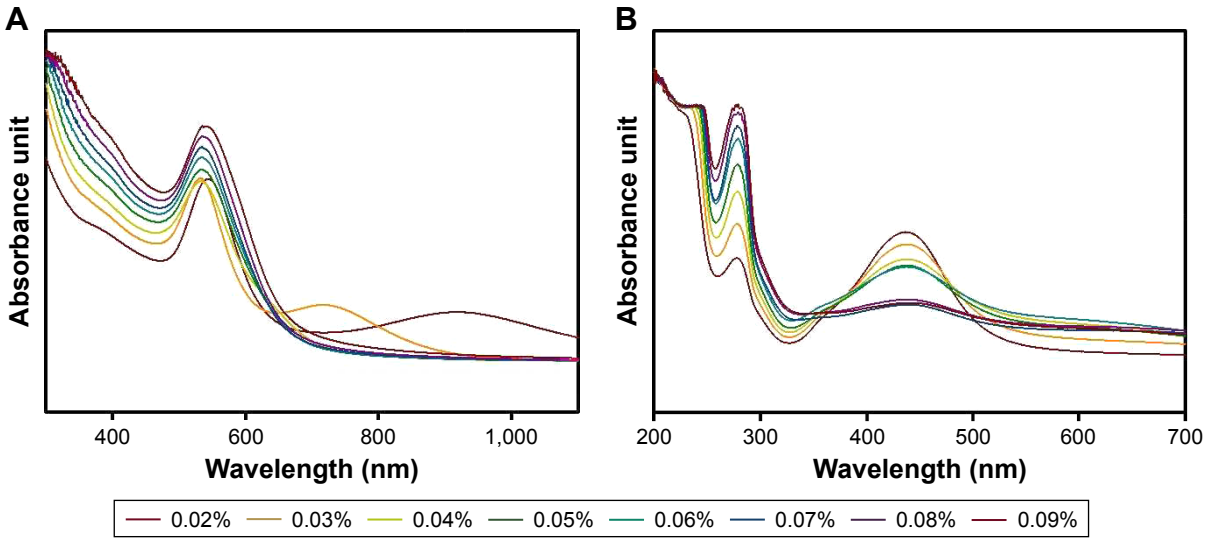

Figure 1 UV-visible spectra of (**A**) GM-AuNPs and (**B**) GM-AgNPs.
Notes: The extract concentration was varied from 0.02% to 0.09% (final concentration). For more detailed procedures, please refer to the "Green synthesis of GM-AuNPs and GM-AgNPs" section.
Abbreviations: GM-AgNPs, silver nanoparticles green synthesized by mangosteen pericarp extract; GM-AuNPs, gold nanoparticles green synthesized by mangosteen pericarp extract; UV, ultraviolet.

concentrations (0.02%–0.09%) (Figure 1B). With increasing extract concentration, the absorbance intensity of GM-AgNPs gradually decreased. In contrast, the SPR bands of GM-AuNPs increased with increasing extract concentration.

Hydrodynamic size and zeta potentials

Hydrodynamic size offers information regarding the size of the nanoparticles in aqueous solution. Generally, the hydrodynamic size is larger than that measured from the HR-TEM images, as the hydrodynamic size includes the hydration layer along with the extract on the surface. When the extract concentration was increased, the hydrodynamic size increased (Table 3). For GM-AuNPs, the size increased from 54.6 nm (0.02%) to 132.0 nm (0.09%) (polydispersity index 0.119–0.221), and the size of GM-AgNPs changed from 129.4 nm (0.02%) to 248.5 nm (0.09%) (polydispersity index 0.184–0.253) with increasing extract concentration.

The colloidal stability of nanoparticles is commonly predicted by measuring zeta potentials. Large positive or negative values on the surface demonstrate that large electrostatic repulsive forces between particles increase the colloidal stability. Negative zeta potentials were observed for both types of nanoparticles, as shown in Table 3. There was a clear tendency in the absolute values of the zeta potentials, which decreased with increasing extract concentration in GM-AuNPs from −34.77 mV (0.02%) to −18.92 mV (0.09%). In the case of GM-AgNPs, there was no tendency of the zeta potentials under the variation of extract concentration (−21.17 to −29.02 mV). These results showed that the primary and secondary metabolites of the extract were bound on the surface of the nanoparticles and produced electrostatically stable nanoparticles.

HR-TEM images

HR-TEM images are routinely acquired to visualize nanoparticles. Images provide important information about particle size and shape. Generally, the size of the metallic core can be directly measured from the image. As shown in

Table 3 Average hydrodynamic size and zeta potential values of GM-AuNPs and GM-AgNPs

	Extract concentration (%)	0.02	0.03	0.04	0.05	0.06	0.07	0.08	0.09
GM-AuNPs	Hydrodynamic size (nm)	54.6	72.0	77.2	79.3	81.7	87.8	106.4	132.0
	Polydispersity index	0.208	0.221	0.211	0.207	0.185	0.151	0.139	0.119
	Zeta potential (mV)	−34.77	−34.12	−33.25	−25.04	−24.06	−22.03	−20.43	−18.92
GM-AgNPs	Hydrodynamic size (nm)	129.4	154.5	162.8	166.0	191.2	197.9	201.2	248.5
	Polydispersity index	0.253	0.242	0.237	0.212	0.184	0.204	0.187	0.210
	Zeta potential (mV)	−24.89	−29.02	−25.91	−23.92	−23.23	−24.22	−22.63	−21.17

Abbreviations: GM-AgNPs, silver nanoparticles green synthesized by mangosteen pericarp extract; GM-AuNPs, gold nanoparticles green synthesized by mangosteen pericarp extract.

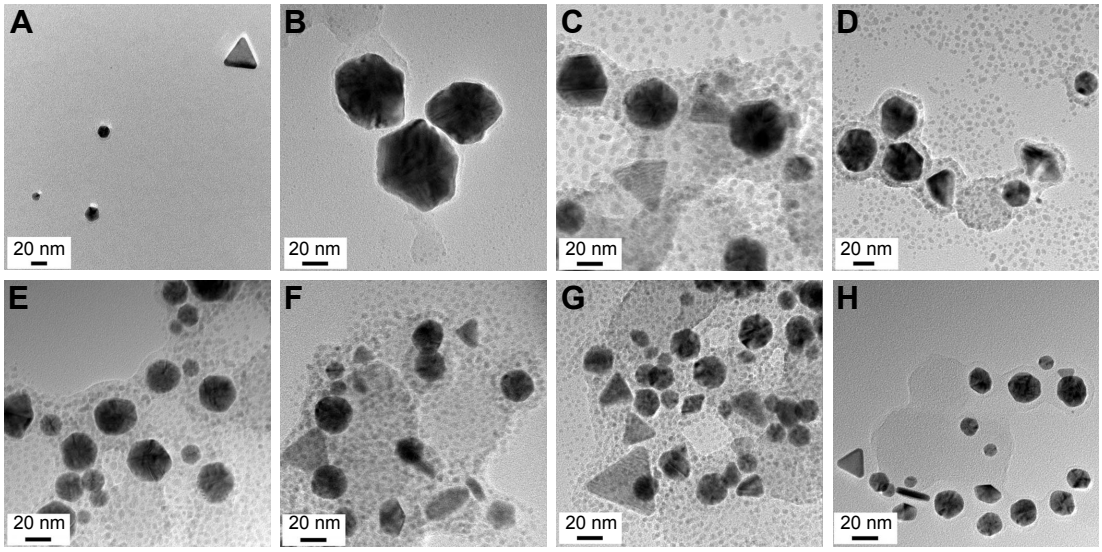

Figure 2 HR-TEM images of GM-AuNPs.
Notes: The extract concentrations utilized for synthesis were (**A**) 0.02%, (**B**) 0.03%, (**C**) 0.04%, (**D**) 0.05%, (**E**) 0.06%, (**F**) 0.07%, (**G**) 0.08%, and (**H**) 0.09%. The scale bar represents 20 nm.
Abbreviations: GM-AuNPs, gold nanoparticles green synthesized by mangosteen pericarp extract; HR-TEM, high-resolution transmission electron microscopy.

Figure 2, the majority of GM-AuNPs were spherical with minor triangular nanoplates.

Most remarkably, asymmetric nanodumbbell homostructures of GM-AgNPs were observed, and representative images are shown in Figure 3. The images acquired of GM-AgNPs synthesized with eight different extract concentrations showed nanodumbbell structures (Figure 3A–H). Nanodumbbells were composed of a silver seed particle (head) with a selective one-sided silver growth of the seed particle (tail). Additionally, we observed two-sided growth of the seed particle (wing), as shown in Figure 3D (red circle); however, the appearance of this wing shape was very rare. The head sizes were directly measured from the image and are summarized in Table 4. The head sizes of nanodumbbells were in the range of 13.65±5.07 to 31.08±3.99 nm. By careful examination of enlarged images (Figure 3G and H), lattice structures were clearly visualized in both the head and tail parts. This result indicated that nanodumbbells were crystalline, which is consistent with the result from HR-XRD in the following section. The distance between two neighboring lattice fringes was measured to

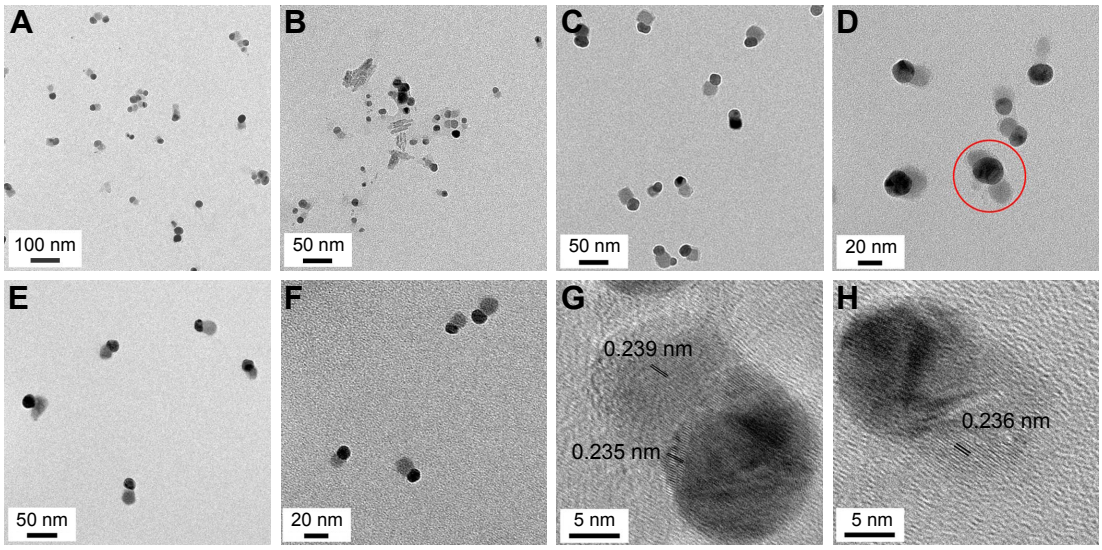

Figure 3 HR-TEM images of GM-AgNPs.
Notes: The extract concentrations utilized for synthesis were (**A**) 0.02%, (**B**) 0.09%, (**C**) 0.08%, (**D**) 0.03%, (**E**) 0.09%, (**F**) 0.05%, (**G**) 0.03%, and (**H**) 0.02%. A red circle (**D**) shows a silver seed particle (head) with two-sided growth (wing); however, the appearance of this wing shape was very rare. The distance between two neighboring lattice fringes was measured to be 0.235 nm for heads and 0.236 nm and 0.239 nm for tails (**G** and **H**).
Abbreviations: GM-AgNPs, silver nanoparticles green synthesized by mangosteen pericarp extract; HR-TEM, high-resolution transmission electron microscopy.

Table 4 Average size of GM-AuNPs and GM-AgNPs measured from HR-TEM images

Extract concentration (%)	0.02	0.03	0.04	0.05	0.06	0.07	0.08	0.09
GM-AuNPs (nm)	31.23±11.89 (14)	44.20±16.99 (57)	38.61±8.43 (22)	30.48±6.88 (7)	25.40±8.62 (38)	20.67±6.83 (19)	18.71±6.41 (81)	15.37±3.99 (44)
GM-AgNPs (nm)[a]	27.78±4.05 (100)	19.33±3.22 (84)	20.96±2.55 (48)	14.13±2.75 (66)	31.08±3.99 (10)	13.65±5.07 (102)	20.14±2.84 (89)	14.35±3.15 (75)

Notes: [a]The head size of nanodumbbells was measured. The number in the parenthesis indicates nanoparticle numbers which were randomly selected from HR-TEM images for size measurements.
Abbreviations: GM-AgNPs, silver nanoparticles green synthesized by mangosteen pericarp extract; GM-AuNPs, gold nanoparticles green synthesized by mangosteen pericarp extract; HR-TEM, high-resolution transmission electron microscopy.

be 0.235 nm for heads and 0.236 nm and 0.239 nm for tails (Figure 3G and H), suggesting that the predominant plane of the crystalline structure was the (111) plane. By careful examination of HR-XRD pattern as discussed in the following section, the (111) plane was found to be the most intense peak. Thus, both HR-TEM and HR-XRD findings corroborated each other well. Zhang et al[25] reported asymmetric nanodumbbell heterostructures composed of AgBr cores with silver tails. In the present report, the Ag nanodumbbell homostructures were synthesized; therefore, further study will be needed to understand the synthetic mechanism.

Characterization of GM-AuNPs and GM-AgNPs synthesized with 0.02% extract concentration

As mentioned in the previous section, we selected the lowest extract concentration (0.02%) to synthesize both nanoparticles for further characterization, in vitro cytotoxicity, and apoptosis. Digital images in the inset present the color of colloidal solutions of each nanoparticle that were synthesized with 0.02% extract concentration (Figure 4). GM-AuNPs showed a wine red color and GM-AgNPs displayed a yellow color after the synthesis, suggesting that each nanoparticle was successfully synthesized. The SPR signals of GM-AuNPs and GM-AgNPs were observed at 544 and 437 nm, respectively (Figure 4). The hydrodynamic size was measured to be 54.6 and 129.4 nm for GM-AuNPs and GM-AgNPs, respectively (Figure 5).

Subsequently, the crystalline nature was confirmed by analyzing the HR-XRD pattern (Figure 6). Strong diffraction peaks at 38.4°, 44.6°, 64.9°, and 77.5° of GM-AuNPs corresponded to the (111), (200), (220), and (311) planes, respectively, of the Au crystal (Figure 6A). In the case of GM-AgNPs, strong diffraction peaks were observed at 38.2°, 44.2°, and 64.5°, corresponding to the (111), (200), and (220) planes of the Ag crystal (Figure 6B). These results suggested that both nanoparticles possessed a face-centered cubic structure. Careful examination of peaks indicated that the (111) plane had the highest intensity, suggesting that the (111) plane was a major orientation of both types of nanoparticles. Thus, we employed the Scherrer equation ($D = 0.89\lambda/W\cos\theta$) to estimate a rough size from the (111) peak. Each term in the equation is defined as follows: D is the particle size, λ is the wavelength of X-ray used, θ is the Bragg diffraction angle, and β is the full width at half maximum of the (111) peak in radians. The estimated size was 27.73 nm for GM-AuNPs and 20.78 nm for GM-AgNPs. From the sizes determined from the HR-TEM images (Table 4),

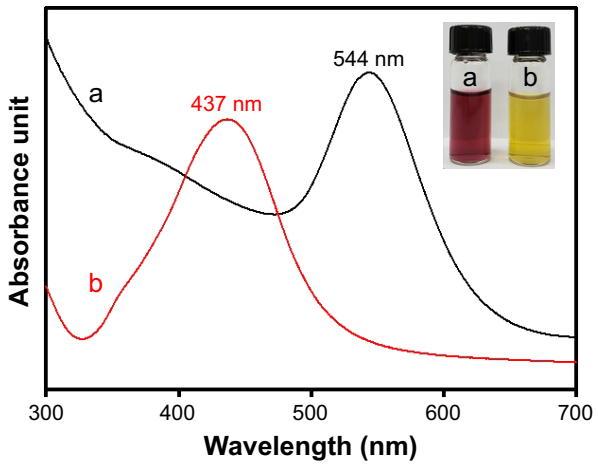

Figure 4 UV-visible spectra of (a) GM-AuNPs and (b) GM-AgNPs.
Notes: Both GM-AuNPs and GM-AgNPs were synthesized with the extract concentration of 0.02%. Digital photographs in the inset show each colloidal solution of GM-AuNPs (left) and GM-AgNPs (right).
Abbreviations: GM-AgNPs, silver nanoparticles green synthesized by mangosteen pericarp extract; GM-AuNPs, gold nanoparticles green synthesized by mangosteen pericarp extract; UV, ultraviolet.

the lowest concentration of the extract (0.02%) produced 31.23±11.89 nm GM-AuNPs and 27.78±4.05 nm GM-AgNPs. The hydrodynamic size was much larger: 54.6 nm for GM-AuNPs and 129.4 nm for GM-AgNPs (Figure 5 and Table 3). There is a discrepancy among these three size measurements (HR-XRD, HR-TEM, and hydrodynamic size). The HR-XRD measurement commonly provides the rough size of the nanoparticles. Both the hydration layer and the biomolecules in the extract on the surface of metallic nanoparticles contributed to the hydrodynamic size; thus, hydrodynamic size is mostly larger than that measured from the HR-TEM images. Only the size of the metallic core is measured from the HR-TEM images.

FT-IR spectra were acquired to obtain information about the functional groups that contributed to the reduction reaction of metal salts to metallic nanoparticles. Three spectra of the extract, GM-AuNPs, and GM-AgNPs are presented in Figure 7. The FT-IR measurements of the extract revealed major bands at 3,295, 2,934, 1,725, 1,607, 1,442, and 1,049 cm^{-1} (Figure 7A). A broad band at 3,295 cm^{-1} indicated the –OH stretching vibration. The existence of hydrogen bonding at –OH groups contributed to broadening the band. The band at 2,934 cm^{-1} represented the $–CH_2$ asymmetric stretching vibration.[26] Ketone (C=O) functional groups appeared at 1,725 cm^{-1}; however, the band intensity was quite weak. The bands at 1,607 and 1,442 cm^{-1} were designated as aromatic C=C bond vibrations.[26] The bond vibrations of C–O and C–H appeared at 1,049 cm^{-1}.[26] The most distinct difference in these spectra was the band from the –OH functional groups. The –OH functional groups in the extract appeared at 3,295 cm^{-1} (Figure 7A), while this band was shifted to 3,211 cm^{-1} in GM-AuNPs (Figure 7B) and 3,341 cm^{-1} in GM-AgNPs (Figure 7C). As demonstrated in the phytochemical screening (Table 1), the extract contained primary and secondary metabolites that were abundant in –OH functional groups, including carbohydrates, flavonoids, glycosides, and phenolic compounds. Therefore, based on the FT-IR spectra and phytochemical screening results, –OH functional groups of the abovementioned primary and secondary metabolites were most likely involved in the synthesis of GM-AuNPs and GM-AgNPs.

Furthermore, the reaction yield was assessed successfully by ICP-OES. After centrifugation of colloidal solution, nanoparticles formed a pellet at the bottom of the tube.

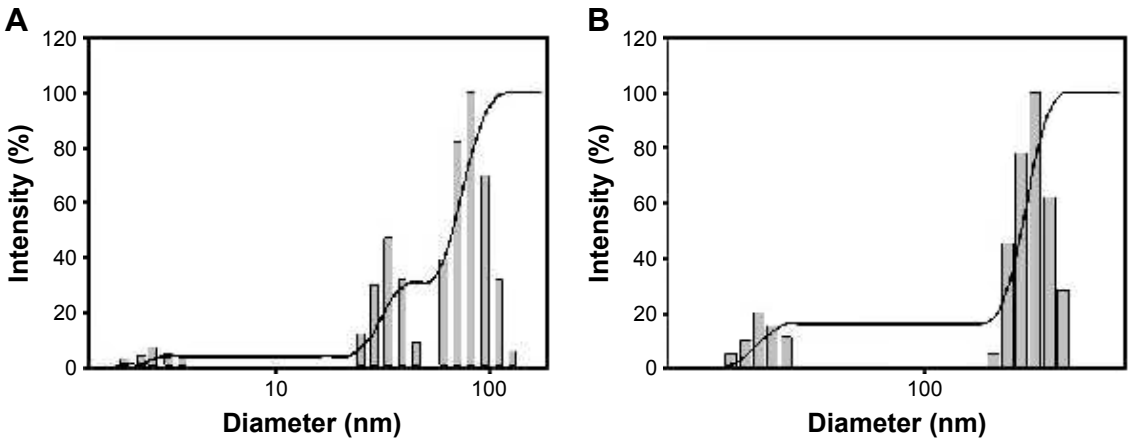

Figure 5 Hydrodynamic sizes of (**A**) GM-AuNPs and (**B**) GM-AgNPs.
Note: Both GM-AuNPs and GM-AgNPs were synthesized with the extract concentration of 0.02%.
Abbreviations: GM-AgNPs, silver nanoparticles green synthesized by mangosteen pericarp extract; GM-AuNPs, gold nanoparticles green synthesized by mangosteen pericarp extract.

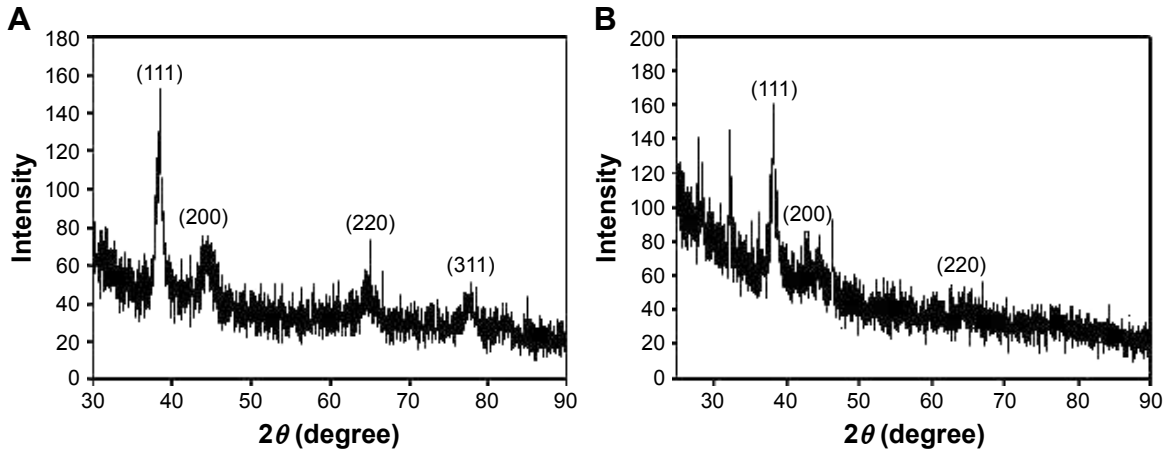

Figure 6 HR-XRD analyses of (**A**) GM-AuNPs and (**B**) GM-AgNPs.
Notes: Both GM-AuNPs and GM-AgNPs were synthesized with the extract concentration of 0.02%.
Abbreviations: GM-AgNPs, silver nanoparticles green synthesized by mangosteen pericarp extract; GM-AuNPs, gold nanoparticles green synthesized by mangosteen pericarp extract; HR-XRD, high-resolution X-ray diffraction.

The supernatant contained an unreacted Au ion or Ag ion. The total Au or Ag concentration was obtained by analyzing the initial colloidal solution. Based on ICP-OES analysis, the reaction yields of GM-AuNPs and GM-AgNPs were 99.7% and 82.8%, respectively. The reaction yield of GM-AuNPs was higher than that of GM-AgNPs.

In vitro cytotoxicity studies of GM-AuNPs and GM-AgNPs on A549 and NIH3T3 cells

The cytotoxicity results using the WST assay were demonstrated on the A549 cells after 24 h of incubation (Figure 8A). The substantial cytotoxicity of GM-AgNPs was observed at 18.75, 37.5, and 75.0 μg/mL. The cytotoxicity of GM-AgNPs at 18.75 μg/mL was 11.9%. From the extract, the significant cytotoxicity was measured at 37.5 and 75.0 μg/mL. The cytotoxicity of the extract at 37.5 μg/mL was 12.7%. However, GM-AuNPs showed cytotoxicity at the highest concentration 75.0 μg/mL (23.5% cytotoxicity). Next, the cytotoxicity of GM-AuNPs and GM-AgNPs was evaluated on NIH3T3 cells after 24 h of incubation (Figure 8B). At 37.5 μg/mL, GM-AuNPs conferred 98.0% cell viability, whereas GM-AgNPs represented 63.0% cytotoxicity. Most interestingly, GM-AuNPs showed cell viability of 93.8% at a concentration as high as 75 μg/mL.

These results suggested that GM-AgNPs showed potent cytotoxicity to both cells. Meanwhile, the cell viability of GM-AuNPs was higher than that of the extract on both cells at all tested concentrations. The results strongly suggested that GM-AuNPs can be potential carriers for delivering drugs and bioactive molecules. Similar results were observed by Abbai et al[26] when they green synthesized both AuNPs and AgNPs using the extract of Siberian ginseng (*Eleutherococcus senticosus*). AgNPs were toxic to MCF7 (a human breast cancer cell) and only slightly toxic to HaCaT (a human keratinocyte cell), while AuNPs were not toxic to either cell.[26]

Observation of cell morphology

The cell morphological changes upon the treatment of three samples (ie, the extract, GM-AuNPs, and GM-AgNPs) are shown in Figure 9. After treatment of GM-AuNPs, as shown in Figure 9C (A549 cells) and Figure 9G (NIH3T3 cells), GM-AuNPs entered the cells and aggregated as red particles that were clearly visible. However, the morphology of GM-AuNP-treated cells did not change significantly when compared with the vehicles (Figure 9A and E). This result implied that GM-AuNPs possessed low cytotoxicity and good biocompatibility, which well correlated with cytotoxicity results in the previous section. Nam et al[27] have reported the use of aggregated AuNPs for photothermal cancer therapy with a low-dose laser irradiation. In the current report, GM-AuNPs entered A549 cells and aggregated themselves (Figure 9C). This result implied that GM-AuNPs have the potential in the applications of photothermal cancer therapy. A detailed study will be required for photothermal cancer therapy of GM-AuNPs in the near future. However, the cells treated with GM-AgNPs showed dead cells and apoptotic bodies indicating low viability, especially in the NIH3T3 cells (Figure 9D and H).

Annexin V/PI staining

Morphological changes were evidently visualized with the treatment of GM-AgNPs on both cells. Thus, in order

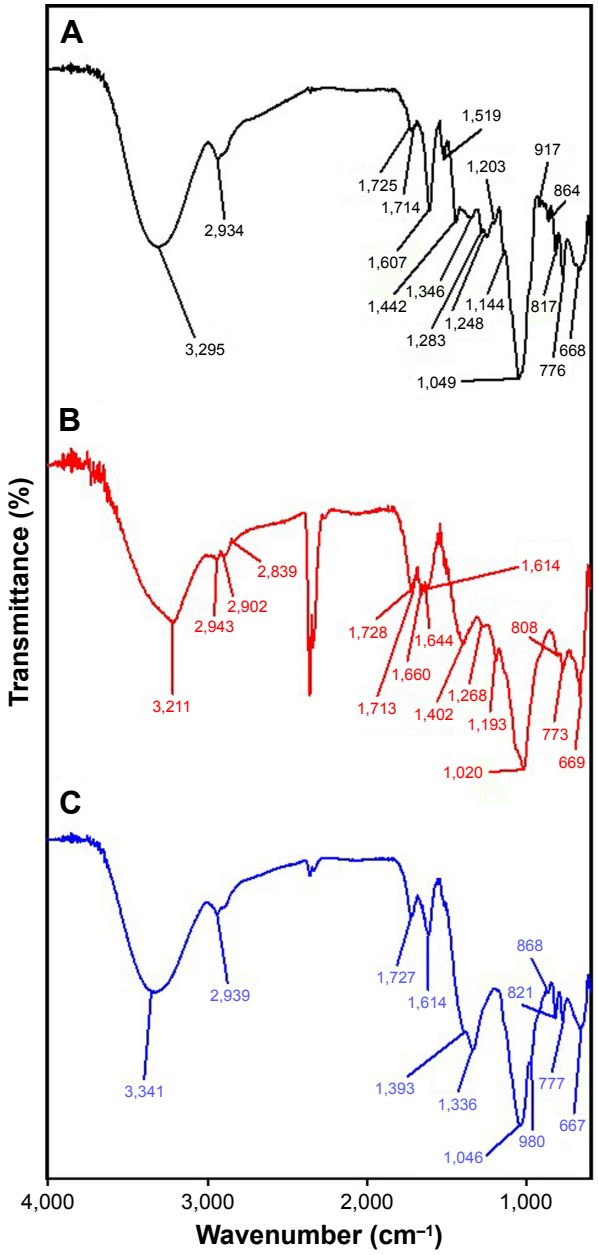

Figure 7 FT-IR spectra of (**A**) the extract, (**B**) GM-AuNPs, and (**C**) GM-AgNPs.
Note: Both GM-AuNPs and GM-AgNPs were synthesized with the extract concentration of 0.02%.
Abbreviations: FT-IR, Fourier transform infrared spectroscopy; GM-AgNPs, silver nanoparticles green synthesized by mangosteen pericarp extract; GM-AuNPs, gold nanoparticles green synthesized by mangosteen pericarp extract.

to investigate whether or not cell death and morphological changes were initiated from apoptosis, Annexin V/PI staining followed by analyzing with FACS was conducted to the treated cells (Figure 10). On A549 cells, the percentage of early apoptosis was observed to be 0.90% for vehicles, 2.51% for the extract, 1.58% for GM-AuNPs, and 33.09% for GM-AgNPs. For NIH3T3 cells, the percentage of early apoptosis was observed to be 0.41% for vehicles, 0.92% for the extract, 0.47% for GM-AuNPs, and 12.08% for GM-AgNPs. GM-AgNPs induced late apoptosis and cell death. In addition, early apoptosis of GM-AgNPs increased in a dose-dependent manner from 18.75 to 75 µg/mL on A549 cells (data not shown). These results clearly demonstrated that GM-AgNPs efficiently induced cell apoptosis on A549 cells. As shown in Figure 11, after the treatment of GM-AgNPs on A549 cells, the percentage of early apoptosis (lower right quadrant in flow cytometric analysis) was 33.09%, which was a major indication of cell death. Interestingly, at concentration of 37.5 µg/mL, GM-AuNPs exhibited better cell viability than that of the extract (Figure 8). This result well correlated with apoptosis result (Figure 10); the percentage of early apoptosis of GM-AuNPs was lower than that of the extract (Figure 11).

Conclusion

Currently, nanomaterials are a new strategy for cancer therapy to overcome multidrug resistance and the side effects of traditional therapy. Among the diverse nanomaterials studied, such as AuNPs, polymeric nanoparticles, carbon-based materials, iron oxide nanoparticles, cerium oxide nanoparticles, and quantum dots, metallic nanoparticles have been widely used for diagnostic and therapeutic applications.[28] Metallic nanoparticles can be easily synthesized, and their surface modification is facile. Furthermore, the scale-up process is relatively simple. With emerging sustainability initiatives, diverse plant extracts can play the role of a reducing agent to synthesize metallic nanoparticles, that is, to convert metallic ions to nanoparticles. People consume the mangosteen aril as a food source, and its pericarp is a waste. Thus, in the present report, the use of pericarp waste to produce valuable nanoparticles was driven by sustainability initiatives. Mangosteen pericarp extract was successfully employed as a reducing agent for the synthesis of GM-AuNPs and GM-AgNPs. Both nanoparticles were characterized using UV-visible spectrophotometry, HR-TEM, HR-XRD, FT-IR, ICP-OES, hydrodynamic size, and zeta potential measurements. Spherical GM-AuNPs and asymmetric dumbbell-shaped GM-AgNPs were observed under HR-TEM images. The WST assay indicated that GM-AgNPs showed cytotoxicity toward both A549 and NIH3T3 cells. On A549 cells, the cytotoxicity of GM-AgNPs was associated with apoptotic programed cell death. Many other researchers also have reported the cytotoxicity of green-synthesized AgNPs on lung cancer cells.[29,30] Wang et al[29] reported green-synthesized AgNPs by *Dendropanax morbifera* leaf extract, and the AgNPs showed potent cytotoxicity toward the A549 cells. The extract of *Dimocarpus*

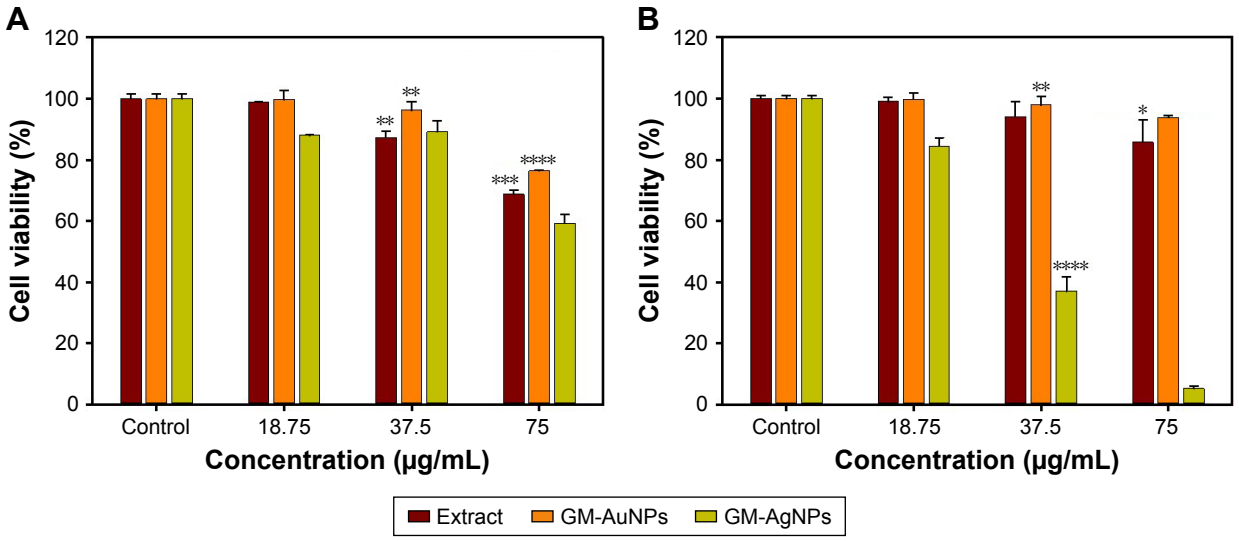

Figure 8 In vitro cytotoxicity of (**A**) A549 cells and (**B**) NIH3T3 cells treated with the extract, GM-AuNPs, and GM-AgNPs.
Notes: The concentration was expressed as the extract concentration. All experiments were performed in triplicate, and all data were presented as mean ± standard deviation. Student's *t*-test was performed to compare the mean values of the two sessions. Asterisks represent statistical difference between control and sample treated groups (*$P<0.05$; **$P<0.01$; ***$P<0.001$; and ****$P<0.0001$).
Abbreviations: GM-AgNPs, silver nanoparticles green synthesized by mangosteen pericarp extract; GM-AuNPs, gold nanoparticles green synthesized by mangosteen pericarp extract.

longan was utilized for the synthesis of AgNPs by He et al,[30] and the AgNPs showed significant cytotoxicity toward the H1299 human lung cancer cells.

Interestingly, asymmetric dumbbell-shaped GM-AgNPs (13.65±5.07 to 31.08±3.99 nm) synthesized in the present report demonstrated higher cytotoxicity on A549 cells than spherical AgNPs with a similar size.[31,32] On A549 cells, GM-AgNPs showed a cytotoxicity of 40.7% at 37.5 μg/mL (based on the extract concentration). At this concentration, Ag concentration was 14.16 μg/mL, determined by ICP-OES. When compared with the previous report, more than two-fold Ag concentration (32.33 μg/mL) was needed to show 40% cytotoxicity on A549 cells with spherical-shaped 10 nm-AgNPs.[33] Therefore, asymmetric dumbbell-shaped

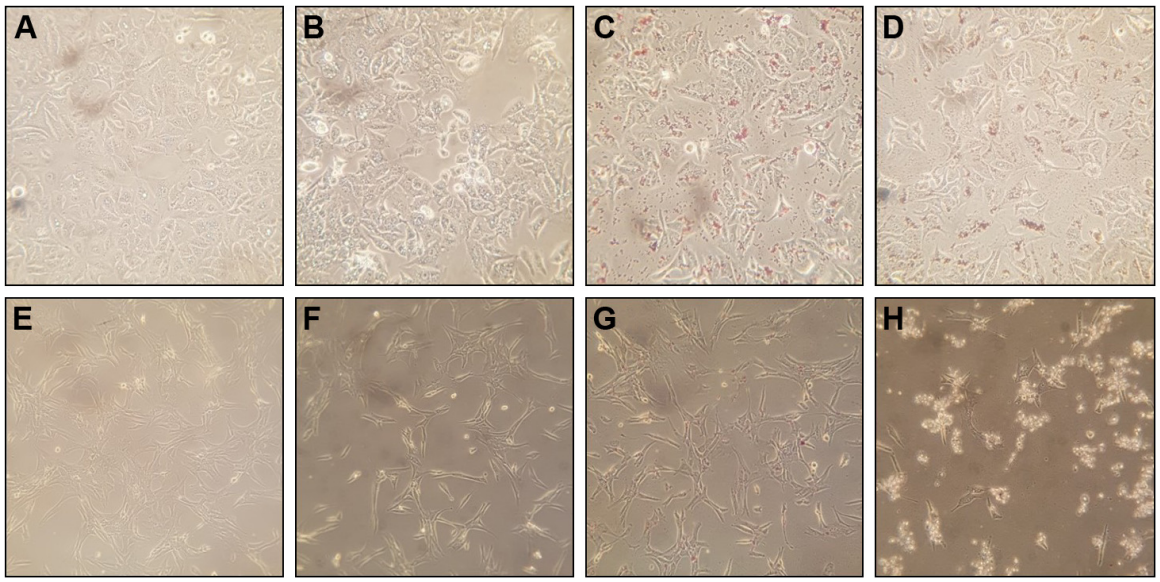

Figure 9 Morphological changes of A549 cells (**A**–**D**) and NIH3T3 cells (**E**–**H**) under light microscopy at the magnification of 200×.
Notes: A549 cells were treated with (**A**) vehicles, (**B**) the extract, (**C**) GM-AuNPs, and (**D**) GM-AgNPs. NIH3T3 cells were treated with (**E**) vehicles, (**F**) the extract, (**G**) GM-AuNPs, and (**H**) GM-AgNPs. The cells were treated with three samples (ie, extract, GM-AuNPs, and GM-AgNPs) the concentrations of which were 37.5 μg/mL (based on the extract concentration).
Abbreviations: GM-AgNPs, silver nanoparticles green synthesized by mangosteen pericarp extract; GM-AuNPs, gold nanoparticles green synthesized by mangosteen pericarp extract.

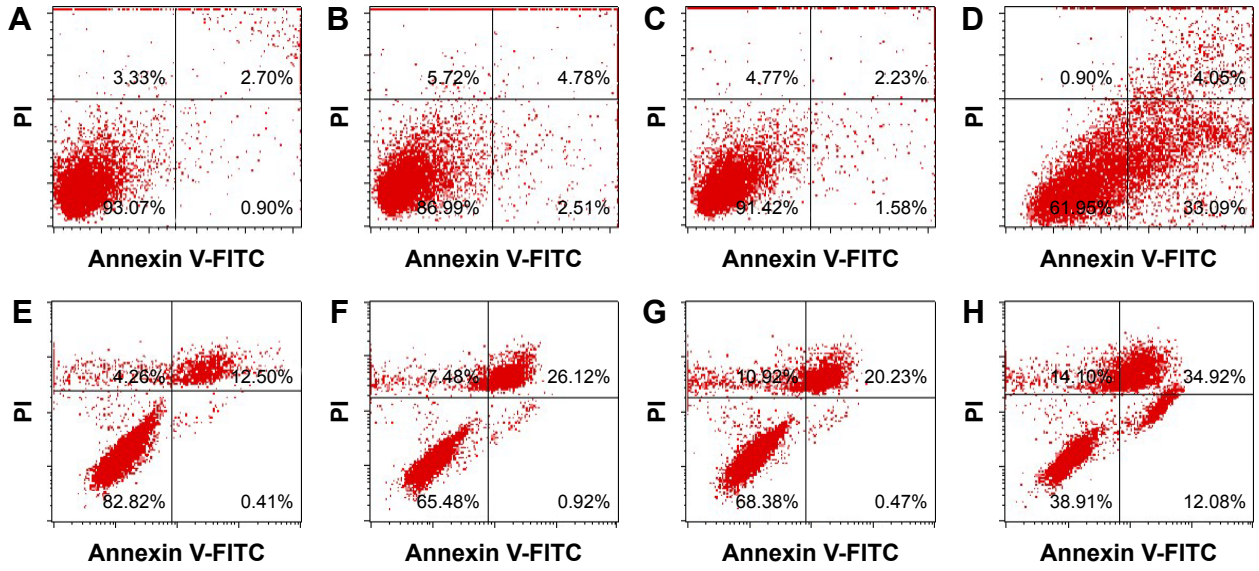

Figure 10 Measurement of apoptotic population induced by the extract, GM-AuNPs, and GM-AgNPs on A549 cells (**A**–**D**) and NIH3T3 cells (**E**–**H**).
Notes: A549 cells were treated with (**A**) vehicles, (**B**) the extract, (**C**) GM-AuNPs, and (**D**) GM-AgNPs. NIH3T3 cells were treated with (**E**) vehicles, (**F**) the extract, (**G**) GM-AuNPs, and (**H**) GM-AgNPs. The cells were treated with three samples (ie, extract, GM-AuNPs, and GM-AgNPs) the concentrations of which were 37.5 μg/mL (based on the extract concentration). The lower left quadrant, lower right quadrant, and upper right quadrant represent living cells, early apoptosis, and late apoptosis (and dead cells), respectively.
Abbreviations: FITC, fluorescein isothiocyanate; GM-AgNPs, silver nanoparticles green synthesized by mangosteen pericarp extract; GM-AuNPs, gold nanoparticles green synthesized by mangosteen pericarp extract.

GM-AgNPs were more cytotoxic on A549 cells than the spherical ones, suggesting that the shape of AgNPs is an important factor for cancer cytotoxicity.

In the case of AuNPs, a wide array of applications has emerged, such as carriers for drug delivery, photothermal therapy, photodynamic therapy, catalysis, sensing, and imaging.[34] Specifically, AuNPs are very popular as delivery vehicles due to their low cytotoxicity, facile synthesis, good biocompatibility, high tissue permeability, spherical shape with uniform size, and relatively simple surface modifications. In the present report, GM-AuNPs did not exert any significant cytotoxicity on both cells. GM-AuNP treatment did not affect cell morphology notably, which further confirmed excellent biocompatibility of GM-AuNPs. Therefore, it can be concluded that GM-AuNPs that were green-synthesized with mangosteen pericarp extract are effective drug delivery carriers for diagnostic and therapeutic applications. Additionally, the treatment of GM-AuNPs on A549 cells caused the aggregation of AuNPs. This phenomenon can be applied for photothermal cancer therapy of GM-AuNPs. In summary, the extract of mangosteen pericarp waste is a valuable natural source to produce prospective metallic nanoparticles possessing effective biological activities.

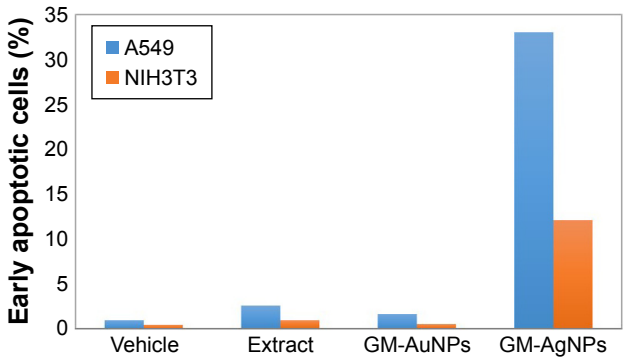

Figure 11 The percentages of early apoptotic cells on both A549 and NIH3T3 cells were quantified with a treatment of 37.5 μg/mL concentration of the samples (based on the extract concentration).
Abbreviations: GM-AgNPs, silver nanoparticles green synthesized by mangosteen pericarp extract; GM-AuNPs, gold nanoparticles green synthesized by mangosteen pericarp extract.

Acknowledgment

This work was supported by the National Research Foundation of Korea (NRF) through a grant funded by the Korean Government by the Ministry of Education (NRF-2015R1D1A1A09059054).

Disclosure

The authors report no conflicts of interests in this work.

References

1. Sasidharan A, Monteiro-Riviere NA. Biomedical applications of gold nanomaterials: opportunities and challenges. *Wiley Interdiscip Rev Nanomed Nanobiotechnol*. 2015;7(6):779–796.

2. Priyadarshini E, Pradhan N. Gold nanoparticles as efficient sensors in colorimetric detection of toxic metal ions: a review. *Sens Actuators B Chem*. 2017;238:888–902.
3. Mikami Y, Dhakshinamoorthy A, Alvaro M, Garcia H. Catalytic activity of unsupported gold nanoparticles. *Catal Sci Technol*. 2013;3(1):58–69.
4. Ahmed S, Ahmad M, Swami BL, Ikram S. A review on plants extract mediated synthesis of silver nanoparticles for antimicrobial applications: a green expertise. *J Adv Res*. 2016;7(1):17–28.
5. Duran N, Duran M, de Jesus MB, Seabra AB, Favaro WJ, Nakazato G. Silver nanoparticles: a new view on mechanistic aspects on antimicrobial activity. *Nanomedicine*. 2016;12(3):789–799.
6. Park Y, Hong YN, Weyers A, Kim YS, Linhardt RJ. Polysaccharides and phytochemicals: a natural reservoir for the green synthesis of gold and silver nanoparticles. *IET Nanobiotechnol*. 2011;5(3):69–78.
7. Suttirak W, Manurakchinakorn S. *In vitro* antioxidant properties of mangosteen peel extract. *J Food Sci Technol*. 2014;51(12):3546–3558.
8. Obolskiy D, Pischel I, Siriwatanametanon N, Heinrich M. *Garcinia mangostana* L.: a phytochemical and pharmacological review. *Phytother Res*. 2009;23(8):1047–1065.
9. Veerasamy R, Xin TZ, Gunasagaran S, et al. Biosynthesis of silver nanoparticles using mangosteen leaf extract and evaluation of their antimicrobial activities. *J Saudi Chem Soc*. 2011;15(2):113–120.
10. Karthiga P, Soranam R, Annadurai G. Alpha-mangostin, the major compound from *Garcinia mangostana* Linn. responsible for synthesis of Ag nanoparticles: its characterization and evaluation studies. *Res J Nanosci Nanotechnol*. 2012;2(2):46–57.
11. Rajakannu S, Shankar S, Perumal S, Subramanian S, Dhakshinamoorthy GP. Biosynthesis of silver nanoparticles using *Garcinia mangostana* fruit extract and their antibacterial, antioxidant activity. *Int J Curr Microbiol Appl Sci*. 2015;4(1):944–952.
12. Pan-In P, Wanichwecharungruang S, Hanes J, Kim AJ. Cellular trafficking and anticancer activity of *Garcinia mangostana* extract-encapsulated polymeric nanoparticles. *Int J Nanomedicine*. 2014;9:3677–3686.
13. Aisha AFA, Abdulmajid AMS, Ismail Z, Alrokayan SA, Abu-Salah KM. Development of polymeric nanoparticles of *Garcinia mangostana* xanthones in eudragit RL100/RS100 for anti-colon cancer drug delivery. *J Nanomater*. 2015;2015:701979.
14. Pan-in P, Tachapruetinun A, Chaichanawongsaroj N, Banlunara W, Suksamrarn S, Wanichwecharungruang S. Combating *Helicobacter pylori* infections with mucoadhesive nanoparticles loaded with *Garcinia mangostana* extract. *Nanomedicine*. 2014;9(3):457–468.
15. Tiwari P, Kumar B, Kaur M, Kaur G, Kaur H. Phytochemical screening and extraction: a review. *Int Pharm Sciencia*. 2011;1(1):98–106.
16. Hossain MA, AL-Raqmi KAS, AL-Mijizy ZH, Weli AM, Al-Riyami Q. Study of total phenol, flavonoids contents and phytochemical screening of various leaves crude extracts of locally grown *Thymus vulgaris*. *Asian Pac J Trop Biomed*. 2013;3(9):705–710.
17. Chanda S, Dave R. In vitro models for antioxidant activity evaluation and some medicinal plants possessing antioxidant properties: an overview. *Arf J Microbiol Res*. 2009;3(13):981–996.
18. Gusakov AV, Kondratyeva EG, Sinitsyn AP. Comparison of two methods for assaying reducing sugars in the determination of carbohydrase activities. *Int J Anal Chem*. 2011;2011:283658.
19. Pratap CR, Vysakhi MV, Manju S, Kannan M, Abdul KS, Sreekumaran NA. *In vitro* free radical scavenging activity of aqueous and methanolic leaf extracts of *Aegle tamilnadensis* (Rutaceae). *Int J Pharm Pharm Sci*. 2013;5(suppl 3):819–823.
20. Zheleva-Dimitrova D, Nedialkove P, Kitanov G. Radical scavenging and antioxidant activities of methanolic extracts from *Hypericum* species growing in Bulgaria. *Pharmacogn Mag*. 2010;6(22):74–78.
21. Parul R, Saha P, Kundu SK. In vitro nitric oxide scavenging activity of methanol extracts of three Bangladeshi medicinal plants. *Pharma Innov*. 2012;1(12):83–88.
22. Babu D, Gurumurthy P, Borra SK, Cherian KM. Antioxidant and free radical scavenging activity of triphala determined by using different in vitro models. *J Med Plant Res*. 2013;7(39):2898–2905.
23. Vermes I, Haanen C, Steffens-Nakken H, Reutelingsperger C. A novel assay for apoptosis flow cytometric detection of phosphatidylserine expression on early apoptotic cells using fluorescein labelled expression on Annexin V. *J Immunol Methods*. 1995;184(1):39–51.
24. Shahidi F, Ambigaipalan P. Phenolics and polyphenolics in foods, beverages and spices: antioxidant activity and health effects–a review. *J Funct Foods*. 2015;18(pt B):820–897.
25. Zhang H, Cao L, Liu W, Su G, Gao R, Zhao Y. The key role of nanoparticle seeds during site-selective growth of silver to fabricate core-shell or asymmetric dumbbell heterostructures. *Dalton Trans*. 2014;43(12):4822–4829.
26. Abbai R, Mathiyalagan R, Markus J, et al. Green synthesis of multifunctional silver and gold nanoparticles from the oriental herbal adaptogen: Siberian ginseng. *Int J Nanomedicine*. 2016;11:3131–3143.
27. Nam J, Won N, Jin H, Chung HK, Kim S. pH-induced aggregation of gold nanoparticles for photothermal cancer therapy. *J Am Chem Soc*. 2009;131(38):13639–13645.
28. Huang Y, Fan CQ, Dong H, Wang SM, Yang XC, Yang SM. Current applications and future prospects of nanomaterials in tumor therapy. *Int J Nanomedicine*. 2017;12:1815–1825.
29. Wang C, Mathiyalagan R, Kim YJ, et al. Rapid green synthesis of silver and gold nanoparticles using *Dendropanax morbifera* leaf extract and their anticancer activities. *Int J Nanomedicine*. 2016;11:3691–3701.
30. He Y, Du Z, Ma S, et al. Effects of green-synthesized silver nanoparticles on lung cancer cells in vitro and grown as xenograft tumors in vivo. *Int J Nanomedicine*. 2016;11:1879–1887.
31. Kanipandian N, Thirumurugan R. A feasible approach to phyto-mediated synthesis of silver nanoparticles using industrial crop *Gossypium hirsutum* (cotton) extract as stabilizing agent and assessment of its in vitro biomedical potential. *Ind Crops Prod*. 2014;55:1–10.
32. Chairuangkitti P, Lawanprasert S, Roytrakul S, et al. Silver nanoparticles induce toxicity in A549 cells via ROS-dependent and ROS-independent pathways. *Toxicol In Vitro*. 2013;27(1):330–338.
33. Jeong JK, Gurunathan S, Kang MH, et al. Hypoxia-mediated autophagic flux inhibits silver nanoparticle-triggered apoptosis in human lung cancer cells. *Sci Rep*. 2016;6:21688.
34. Sperling RA, Gil PR, Zhang F, Zanella M, Parak WJ. Biological applications of gold nanoparticles. *Chem Soc Rev*. 2008;37(9):1896–1908.